# PONTIFICIA UNIVERSIDAD CATÓLICA DEL PERÚ

## FACULTAD DE CIENCIAS E INGENIERÍA


# Propagation of Exothermic Reaction Fronts in Liquids

Tesis para optar al Título de Licenciado en Física, que presenta el bachiller

**David Reinaldo Alejandro Ruelas Paredes**

**ASESOR: Desiderio A. Vásquez Rodríguez**

Lima, Marzo de 2016

# Propagation of Exothermic Reaction Fronts in Liquids

**David Reinaldo Alejandro Ruelas Paredes**

Propuesto para el Título de Licenciado en Física

2016

## Resumen

La convección es el proceso en el que los fluidos menos densos se elevan sobre otros más densos. Se encuentra presente en fenómenos naturales tan diversos como el almacenamiento natural de $CO_2$, la propagación de ondas viajeras, y la formación de columnas de basalto. Por lo tanto, determinar las condiciones bajo las que se produce convección representa un desafío importante. La convección puede originarse por gradientes de densidad debidos a expansión térmica o a cambios de composición en los fluidos. Modelos anteriores y experimentos realizados en la reacción de iodato-ácido arsenioso determinaron que los gradientes del primer tipo producen efectos insignificantes en comparación con los del segundo. Desarrollamos un modelo no-lineal para la propagación de frentes de reacción delgados en reacciones autocatalíticas que ocurren en un sistema bidimensional. Empleamos una ecuación de calor (advección-difusión) para determinar la distribución de temperaturas en el sistema, la ley de Darcy para determinar la velocidad de los fluidos, y la relación eikonal para describir la propagación de los frentes. Los efectos térmicos del modelo dan lugar a frentes planos, no-axisimétricos, y axisimétricos. Sometemos la solución de frente plano de nuestro sistema a un análisis lineal de estabilidad. Para ello introducimos perturbaciones pequeñas, obteniendo así un sistema lineal de ecuaciones para la evolución de dichas perturbaciones. Mediante este análisis determinamos las condiciones para el desarrollo de frentes convectivos. Resumimos estos resultados en el plano generado por nuestros parámetros de control — los números de Rayleigh — y sugerimos posibles usos para este modelo.

# Propagation of Exothermic Reaction Fronts in Liquids

**David Reinaldo Alejandro Ruelas Paredes**

Presented towards a Licentiate's Degree in Physics

2016

## Abstract

Convection, the process in which less dense fluids rise above denser ones, pervades nature: it can be found in phenomena so diverse as natural $CO_2$ storage, propagation of travelling waves, and formation of basalt columns. Determining the conditions under which convection occurs, therefore, poses an alluring challenge. In fluid media, density gradients due to either thermal expansion or changes in composition can ignite convection. Previous models and experiments in the iodate-arsenous acid reaction determined that the former type of gradients were unimportant in comparison to the latter. We develop a nonlinear model for thin fronts propagating in autocatalytic reactions occurring in a two-dimensional system: an advection-diffusion heat equation with a source term to determine the temperature distribution inside the system, Darcy's law to determine how the fluids flow, and the eikonal relation to describe how the fronts propagate. The thermal effects included in our model result in flat, non-axisymmetric, and axisymmetric fronts. We carry out a linear stability analysis of the flat front solution. To this end we introduce small perturbations to said solution, and obtain a linear system of equations that describe how the perturbations grow. This analysis determines the conditions for convective fronts to emerge. We summarize these results in the plane generated by our control parameters — the Rayleigh numbers — and suggest possible uses for our model.

PONTIFICIA UNIVERSIDAD CATÓLICA DEL PERÚ

PONTIFICIA UNIVERSIDAD CATÓLICA DEL PERÚ
Facultad de Ciencias e Ingeniería
17 SET. 2015
MIGUEL MEJIA PUENTE
DECANO

## TEMA DE TESIS

**Para optar:** Título de licenciado en física
**Alumno:** David Reinaldo Alejandro Ruelas Paredes
Código: 20100401

**Propuesto por:** Dr. Desiderio Vásquez
**Asesor:** Dr. Desiderio Vásquez

**Tema: Propagation of exothermic reaction fronts in liquids.**

**N° tema:** 42

**Fecha: 07 de febrero de 2014**

**Descripción del tema y objetivos:**

Experiments in propagation fronts in liquids give rise to fluid motion due to changes in concentrations across the front [1,2]. These changes arise not only from variations in chemical composition between reacted and unreacted fluids, but in some cases they are also due to heat released by the chemical reaction. Such is the case of autocatalytic reaction fronts in the iodate-arsenous acid reaction. The effects of heat release are so important that initial theoretical work found that setting the thermal diffusivity to infinity is an excellent approximation to modeling the convective effects due to thermal composition [3]. Previous experiments in the iodate-arsenous acid reaction showed a transition to convection as a reaction front propagated inside vertical capillary tubes [1]. For tubes of small diameter there was no fluid convection, since ascending reaction fronts had the same speed of descending fronts, with both fronts being flat. However, for larger diameters, ascending fronts were curved moving faster than flat fronts. Increasing the tube diameter further resulted in changing the shape of the propagating front, from non-axisymmetric fronts to axisymmetric fronts. Further experimental work was carried out confining the liquid between two vertical walls in what is referred to as a Hele-Shaw cell [2]. These experiments set an initial flat front following its evolution inside the cell. Buoyancy generated an instability of flat fronts leading to the formation of fingers as the front moved upward. Small perturbations of the flat front grew or decay at different rates.

The experiments used a Fourier decomposition technique to measure the growth rate for perturbations of fixed wavelength. Theoretical work accounted for the transition to convection considering the front as a thin boundary separating reacted and unreacted fluids, with the normal speed of the front determined by an eikonal relation between the flat front speed and the front curvature [4]. Other works they used a reaction-diffusion model which depends of the specific type of reaction. Coupling the reaction-diffusion equations to the heat equation allowed for the analysis of thermal effects[5].

The objective of the present work is to develop a thin front model that includes the analysis of thermal effects. This model is independent of the type of reaction obtaining solutions valid to any autocatalytic reaction front. The front evolution equation will be solved in the small curvature limit. The fluid motion will be modeled using Darcy's law which corresponds to fluid motion inside a Hele-Shaw cell. The heat released will be accounted by a moving delta function located at the position of the front.

**Plan de trabajo**

The fluid dynamic equations (Darcy's law and the mass continuity equation) will be combined to replace the components of the velocity of the fluid with corresponding gradients of a stream function. The resulting Poisson equation will be solved using finite difference techniques on rectangular domain. The variables will be evaluated on grid points separated by a fixed distance. The nonlinear evolution equation will be discretized as well, using a simple Euler method to advance the fronts on a finite time step.

Two important results should be obtained. One is the linear stability analysis for perturbations of fixed wavelength. The growth rate will be calculated as a function of the perturbation wave number. The changes of density will correspond to thermal expansion as well as compositional changes. The second result corresponds to the full solution of the nonlinear equations. As the size of the horizontal domain changes, a transition to convection will take place. The calculations will show transitions between different types of convective fronts.

D. Vargas F. de Zela

PONTIFICIA UNIVERSIDAD CATÓLICA DEL PERÚ

**Referencias y bibliografía básica**


[1] J. Masere, D.A. Vasquez, B.F. Edward, J. W. Wilder, and K. Showalter, "Nonaxisymmetric and Axisymmetric Convection in Propagating Reaction-Diffusion Fronts", J. Phys. Chem. 98, 6505 (1994)

[2] M. Böckmann and S. C. Müller, "Growth Rates of the Buoyancy-Driven Instability of an Autocatalytic Reaction Front in a Narrow Cell", Phys. Rev. Lett. 85, 2506 (2000)

[3] D. A. Vasquez, B. F. Edwards, and J. W. Wilder, "Finite thermal diffusivity at onset of convection in autocatalytic systems: Discontinuous fluid density", Phys. Fluids, 7, 2513 (1995)

[4] D. A. Vasquez, and D. I. Coroian, "Stability of convective patterns in reaction fronts: A comparison of three models", Chaos 20, 033109 (2010).

[5] T. Bánsági, Jr., D. Horváth, Á. Tóth, J. Yang, S. Kalliadasis, and A. De Wit "Density fingering of an exothermic autocatalytic reaction" Phys. Rev. E 68, 055301(R) (2003)

Firma del Asesor

Firma del Coordinador de Especialidad:

# Agradecimientos

En junio del 2013 el profesor Desiderio Vásquez entró al salón de clases y dijo que estaba buscando dos colaboradores para trabajar en sus nuevos proyectos. Al aceptar esta oferta terminé trabajando con él en la investigación que devino en esta tesis de licenciatura. Por haber sido tan oportuno en invitar a sus alumnos a investigar; por haberme aceptado para dicho trabajo; por haberme hecho incontables sugerencias y correcciones a lo largo de la investigación para esta tesis (y en su edición); por haberme apoyado y haber confiado en mí todo este tiempo, le agradezco profundamente al profesor Desiderio.

Todos los profesores que conocí en la universidad, en el colegio, en el instituto de alemán, y en otros lugares contribuyeron muchísimo — de muy diversas formas — en mi desarrollo y aprendizaje. Pese a que probablemente muchos de ellos nunca leerán estas líneas, dejo en ellas constancia de mi deuda con y gratitud hacia ellos.

Mis amigos y compañeros de estudios también fueron (y son) una gran influencia en mí. Sería imposible nombrar a todas estas personas en tan breve espacio y sería injusto nombrar solo a algunas. Por lo tanto, decidí no nombrar a ninguna. Si alguna llega a leer estas líneas y se siente aludida, sepa que estuvo en mi mente a la hora de escribir este párrafo.

Mi familia tomó con algo de escepticismo y sorpresa mi decisión de estudiar Física. No obstante, siempre tuve su apoyo y comprensión. Por más que esto suene solo como un gesto amable de su parte, es mucho más para un adolescente que no está muy seguro de qué hará una vez egrese. Muchas gracias por todo.

Para terminar, el agradecimiento más importante. Mis padres me dieron su apoyo y comprensión desde el instante en que temorosamente les dije que quería cambiarme a Física. Nunca dejaron de animarme, de interesarse por mi futuro, ni de avisarme sobre cada cosa que pensaban podría serme útil. Como si eso no fuera suficiente para estar en deuda con ellos, por muchos años me cuidaron, alimentaron, mantuvieron, acompañaron, y apoyaron — y encima lo siguen haciendo. Papá, mamá: muchas gracias. Este trabajo va para ustedes.

# Contents

# List of Figures

**Chapter 1**



**Chapter 4**

# 1. Introduction

The breadth of complex phenomena that can be studied using relatively simple mathematical models is astonishing: the diffusion equation accounts for the propagation of crime hot spots [1], the Lorenz system simulates forced dissipative flows in the atmosphere [2], the Swift-Hohenberg equation yields patterns of vegetation growth in arid regions [3], the Kuramoto-Daido model describes the synchronization of neural networks [4], and that is just to mention one application per model.

Chemical systems provide a great environment for studying diverse phenomena. In autocatalytic reactions, one of the reactants enhances its own production rate by consuming other reactants. These reactions are exothermic, meaning that they release heat to the surrounding environment [5]–[6]. The complex interplay between chemical reaction and molecular diffusivity creates a moving interface that separates reactants from products — we call this interface reaction front [7]. Reactants and products have different compositions and may be at different temperatures; this leads to density gradients across the front. These gradients generate buoyant forces, which in turn result in the macroscopic fluid flow called convection. Countless natural processes, such as travelling waves [8], basalt fingers formation [9], the genesis of the Moon's early magnetic field [10], and the leakage of natural $CO_2$ storage sources [11], are rooted in convection. This fact motivates studying the conditions under which convection occurs.

One such autocatalytic reaction is the iodate oxidation of arsenous acid. In it both iodide ($I^-$) and iodate ($IO_3{}^-$) ions are present initially; the former species consumes the latter to enhance its own production [12]–[13]. The iodate-arsenous acid reaction has been studied experimentally and theoretically in thin capilar tubes and Hele-Shaw cells, which consist of two plates separated by a small gap that stores reactants and products [14]. The appeal of Hele-shaw cells resides in that they are a good approximation to simpler two-dimensional systems. Theoretical work by Wilder *et al.* [15] as well as experiments by Masere *et al.* [16] established that composition gradients can account entirely for convection in the iodate-arsenous acid reaction. If, however, the thermal and convective lengths of the system are similar — meaning that the temperature decays over the same distance in which convection takes place — the contributions of thermal

gradients affect the onset of convection, as was shown by Vásquez *et al.* [17].

Two types of reaction fronts exist: thin fronts, in which the width that separates reacted and unreacted regions is much smaller than any other length scale in the system, and thick fronts, which exhibit large irregular deformations called fingers. The latter have been extensively studied accounting for heat effects [18] and even heat losses [19]–[20]. Thin fronts can be described with front propagation equations that model different reactions. Studies on thin-front models were carried out without considering heat effects [16] — or considering infinite or zero thermal diffusivity — because previous research had shown that thermal gradients affect the onset of convection significantly less than composition gradients [21].

Aiming to fill in this knowledge gap, we developed and studied a thin-front model that accounts for both thermal and composition density gradients. This model should reproduce previous results in the appropriate limit, which would underscore the importance of heat effects. We obtained our model assuming that the mass continuity equation holds, and that fluid density varies linearly with temperature and has a discontinuous jump at the front due to differences in composition. We also considered the front as a heat source with a curvature smaller than other length scales. It is worth mentioning that we can consider the fluids to be incompressible in using the continuity equation — the changes in density will affect only the large gravity term in the equation for fluid flow.

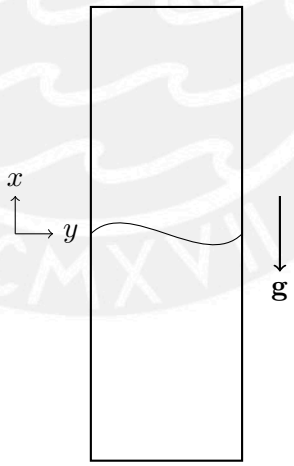


Figure 1.1: The physical system consists of two substances separated by a reaction front. These substances are contained in a very long and narrow tube (not shown to scale) set up vertically in a gravitational field.

The system we studied consists of a long two-dimensional tube standing vertically on a gravitational field, as shown in Fig. 1.1. Since the fluids can only move in a plane, the tube is equivalent to an idealized Hele-Shaw cell. Inside the tube, two substances in aqueous solution undergo an autocatalytic chemical reaction. Although our model can

be applied to many autocatalytic reactions, we focused on the physical and chemical parameters corresponding to the iodate-arsenous acid reaction. The front separating the substances releases heat as it propagates upwards. We described its time evolution in a moving reference frame with the same orientation as the laboratory frame depicted in the diagram.

In Chapter 2 we introduce the nonlinear system of equations that describe the thin-front model, set up a system of nondimensional units, and define appropriate control parameters. We then obtain a convectionless solution for the previous system. To complete our theoretical framework, we carry out a linear stability analysis: we perturb the previous solution and keep only first-order terms. In Chapter 3 we explain the computational algorithms, numerical schemes, and parameters used in the calculations. Chapter 4 presents the results of the nonlinear and linear simulations, which we comment and contrast with previous results. Finally, in Chapter 5 we summarize what we have done, our results, and suggest improvements and possible directions for further research.

# 2. Theoretical background

## 2.1 Nonlinear Model

In developing our nonlinear model, we will use a front propagation equation to describe the evolution of the interface that separates reacted and unreacted fluids. The position of the front will be described with a function $H = H(y,t)$. We will also need two properties of the fluids: their temperature and velocity field. A scalar field $T = T(x,y,t)$ will describe the former and a vector field $\mathbf{v} = \mathbf{v}(x,y,t)$ the latter.

The functional form of the fluid density comprises both thermal and compositional contributions. As the fluids get hotter they undergo volumetric expansion, which we approximate to first order of the corresponding Taylor series. We assume this expansion to be very small. Let $\rho_0$ be the density of the reacted fluid, $T_1$ its temperature, and $\alpha$ the thermal expansion coefficient. The density is given by

$$\rho(x,y,t) = \rho_0 \left[1 - \alpha\left(T - T_1\right) + \beta\Theta(x-H)\right], \quad \text{with } \alpha \equiv -\frac{1}{\rho_0}\left(\frac{\partial\rho}{\partial T}\right)_{T_1}. \tag{2.1}$$

The parameter $\beta$ is the fractional density change between reactants and products, and $\Theta(x-H)$ represents the Heaviside step function, which is defined as

$$\Theta(x-H) = \begin{cases} 0, & \text{if } x < H, \\ 1, & \text{if } x \geq H. \end{cases} \tag{2.2}$$

The fluid velocity field and density satisfy the continuity equation

$$\frac{\partial\rho}{\partial t} + \boldsymbol{\nabla}\cdot\rho\mathbf{v} = 0. \tag{2.3}$$

It encloses the requirement of mass conservation and holds true in particular for our closed system. Following the Boussinesq approximation [22], we assume that density changes will only affect terms that include the gravitational acceleration. This yields the continuity equation for incompressible flow

$$\boldsymbol{\nabla}\cdot\mathbf{v} = 0. \tag{2.4}$$

In electromagnetism, the magnetic field $\mathbf{B}$ satisfies $\boldsymbol{\nabla} \cdot \mathbf{B} = 0$, a condition similar to Eq. 2.4. A simple theorem of vector algebra states that any such vector field can be written as $\mathbf{B} = \boldsymbol{\nabla} \times \mathbf{A}$, where the vector potential $\mathbf{A}$ is not unique [23]. This allows us to eliminate some redundant degrees of freedom in Maxwell's equations — the equations that dictate how the electric and magnetic fields change in space and time due to sources — which in turn makes them easier to solve. This vector-potential formulation of electromagnetism will play a crucial role in our calculations.

We now introduce and describe the main equations of our model:

- Our heat equation is a modified version of the diffusion equation for the material system's temperature. It accounts for three processes: diffusion, the change of $T$ in time due to temperature differences across the system; advection, the macroscopic fluid displacement that transports heat from one region to another; and heat liberation due to a source, the moving front.
- Darcy's law models fluid flow through a porous medium, which is equivalent to the flow inside a Hele-Shaw cell — see, for example, Ref. [11]. It relates these flows to the pressure ($P$) gradient, the fluid density, and gravity.
- The eikonal relation approximates the normal speed of the front as the sum of the flat-front speed $C_0$ — the speed the front would have if it were flat — and the molecular diffusivity $D_C$ multiplied by the front curvature $\mathcal{K} = -\boldsymbol{\nabla} \cdot \hat{\mathbf{n}}$, where $\hat{\mathbf{n}}$ is the unit vector normal to the front, pointing towards the unreacted fluid [24]. This relation holds true only for small curvatures. Since the front propagates in a moving fluid, we couple the normal component of the fluid velocity, $\hat{\mathbf{n}} \cdot \mathbf{v}$, to this equation.

Let $D_T$ denote the thermal diffusivity of the fluids, $\kappa$ their permeability, $\mu$ their viscosity, and $\mathbf{g} = -g\hat{\mathbf{x}}$ gravity. With these considerations in mind, our equations are given by

$$\begin{cases} \dfrac{\partial T}{\partial t} + \mathbf{v} \cdot \boldsymbol{\nabla} T = D_T \nabla^2 T + Q\delta\left(x - H\right), & \text{(2.5a)} \\ \mathbf{v} = -\dfrac{\kappa}{\mu}\left(\boldsymbol{\nabla} P + \rho \mathbf{g}\right), & \text{(2.5b)} \\ C = C_0 + D_C \mathcal{K} + \hat{\mathbf{n}} \cdot \mathbf{v}|_{x=H}. & \text{(2.5c)} \end{cases}$$

Equations 2.5 present us with some difficulties:

- We have introduced a new variable, the pressure, in the description of the fluid flow. Therefore, we would need to include an additional equation — with all the assumptions and requirements it entails — for the pressure's time evolution.
- The eikonal relation, as it stands, requires the computation of the front curvature, which must be obtained from $H$ at every instant. It also obscures the way in which the front evolves.

For these reasons, we must recast the previous equations into a more tractable form. As we will see, this comes at the cost of having to solve slightly more complicated equations, but it will allow us to compute the solutions.

The continuity equation for incompressible flow (Eq. 2.4) allows us to introduce a vector potential $\mathbf{\Psi} = (0, 0, \psi)$, whose $z$-component is the stream function $\psi$. This potential satisfies

$$\boldsymbol{\nabla} \times \mathbf{\Psi} = \mathbf{v} = \left( \frac{\partial \psi}{\partial y}, -\frac{\partial \psi}{\partial x}, 0 \right). \tag{2.6}$$

In this equation, the flow field has been extended to be three-dimensional; we will use only its $x$- and $y$-components in what follows. To eliminate $P$, an irrelevant degree of freedom, we compute the following quantity using first Eq. 2.6 and then Eq. 2.5b:

$$\begin{aligned} \frac{\partial v_x}{\partial y} - \frac{\partial v_y}{\partial x} &= \frac{\partial^2 \psi}{\partial x^2} + \frac{\partial^2 \psi}{\partial y^2} = \nabla^2 \psi \\ &= -\frac{\kappa}{\mu} \left( \frac{\partial^2 P}{\partial y \partial x} + g \frac{\partial \rho}{\partial y} - \frac{\partial^2 P}{\partial x \partial y} \right) = -\frac{\kappa g}{\mu} \frac{\partial \rho}{\partial y}. \end{aligned} \tag{2.7}$$

In accordance with the Boussinesq approximation, we will not neglect the derivative in the right hand side of the last equality. This term can be calculated substituting in the density from Eq. 2.1, which yields a Poisson equation for the stream function:

$$\nabla^2 \psi = \frac{\kappa g \rho_0 \alpha}{\mu} \frac{\partial T}{\partial y} + \frac{\kappa g \rho_0 \beta}{\mu} \frac{\partial H}{\partial y} \delta(x - H). \tag{2.8}$$

The eikonal relation must be rewritten in order to obtain a front evolution equation. Inspecting the system's geometry — and considering the front's boundary conditions, which we discuss below — we find that the normal vector pointing towards the unreacted fluid is given by $(1, -\partial H/\partial y)$. Now we can write the normal speed and curvature in 2.5c as functions of the front's derivatives:

$$\hat{\mathbf{n}} \cdot \hat{\mathbf{x}} \frac{\partial H}{\partial t} = \frac{\partial H/\partial t}{\sqrt{1 + (\partial H/\partial y)^2}} = C_0 + D_C \frac{\partial^2 H/\partial y^2}{[1 + (\partial H/\partial y)^2]^{3/2}} + \hat{\mathbf{n}} \cdot \mathbf{v}|_{x=H}. \tag{2.9}$$

Then, we multiply both sides of the last equality by the square root factor:

$$\frac{\partial H}{\partial t} = C_0 \sqrt{1 + (\partial H/\partial y)^2} + D_C \frac{\partial^2 H/\partial y^2}{1 + (\partial H/\partial y)^2} + v_x - v_y \frac{\partial H}{\partial y}. \tag{2.10}$$

Finally, we approximate the resulting terms using the binomial approximation $(1 + x)^n \approx 1 + nx$ — which is valid if $|x| \ll 1$ — and obtain

$$\frac{\partial H}{\partial t} = C_0 + \frac{C_0}{2} \left( \frac{\partial H}{\partial y} \right)^2 + D_C \frac{\partial^2 H}{\partial y^2} + v_x - v_y \frac{\partial H}{\partial y}, \tag{2.11}$$

where we have neglected the $\mathcal{O}(H^3)$ term. It is worth recalling that in this last equation the components of $\mathbf{v}$ must be computed at $x = H$.

We now introduce the time and length scales $\tau$ and $\ell$. These involve the thermal diffusivity and flat front speed, and are defined as

$$\tau \equiv D_T C_0^{-2} \qquad \text{and} \qquad \ell \equiv D_T C_0^{-1}. \tag{2.12}$$

The non-dimensional flat front speed is then given by $C_0' = C_0/(\ell/\tau) = 1$. We also define a temperature scale as the difference between reacted and unreacted fluid temperatures $\Delta T \equiv T_1 - T_0$ for flat front propagation. With these scales we define a set of primed, dimensionless variables as functions of the original variables:

$$x = x'\ell, \qquad y = y'\ell, \qquad t = t'\tau, \tag{2.13}$$

$$H = H'\ell, \qquad T = T'\Delta T, \qquad \psi = \psi'\ell^2\tau^{-1}. \tag{2.14}$$

After introducing the new variables in the previous equations, dropping the primes, and reordering the new terms, we obtain the nondimensional system

$$\begin{cases} \dfrac{\partial T}{\partial t} + \mathbf{v}\cdot\boldsymbol{\nabla} T = \nabla^2 T + Q\delta\left(x - H\right), & \text{(2.15a)} \\ \nabla^2\psi = \mathrm{Ra_T}\dfrac{\partial T}{\partial y} + \mathrm{Ra_C}\dfrac{\partial H}{\partial y}\delta(x-H), & \text{(2.15b)} \\ \dfrac{\partial H}{\partial t} = C_0 + \dfrac{1}{2}\left(\dfrac{\partial H}{\partial y}\right)^2 + \dfrac{1}{\mathscr{L}}\dfrac{\partial^2 H}{\partial y^2} + v_x - v_y\dfrac{\partial H}{\partial y}. & \text{(2.15c)} \end{cases}$$

In Eq. 2.15c we have introduced the Lewis number, $\mathscr{L} \equiv D_T/D_C$, which characterizes the chemical reaction of interest. The change of scales gives us two important dimensionless parameters that measure the intensity of thermal and composition gradients: the thermal and composition Rayleigh numbers

$$\mathrm{Ra_T} \equiv \frac{\kappa g \rho_0 \tau \alpha \Delta T}{\mu \ell} \qquad \text{and} \qquad \mathrm{Ra_C} \equiv \frac{\kappa g \rho_0 \tau \beta}{\mu \ell}. \tag{2.16}$$

In what follows, all quantities will be nondimensional unless dimensions are explicitly indicated.

To complete our prescription for solving the nonlinear model we must impose appropriate boundary conditions. The front is an impermeable boundary that separates reacted and unreacted fluids. As a consequence, the derivative with respect to $y$ of the front height function $H(y,t)$ must equal zero at $y = 0$ and $y = Ly$. The initial conditions for both $T$ and $H$ are small perturbations about $0$. We assumed that the top of the tube is cooled — accounting for the fact that it is far away from the heat source: the front — so that $T(x = Lx, y, t) = 0$. At the other boundaries we impose no-penetration boundary conditions, i.e. $\hat{\mathbf{n}}\cdot\boldsymbol{\nabla} T = 0$, meaning that heat does not flow into or out of the tube. By the same token, the velocity field must also satisfy no-penetration boundary conditions. To ensure that it does, we set the stream function equal to zero at the boundaries.

## 2.2 Zeroth-Order Solution

In absence of convection, the solution of Eq. 2.15c corresponds to a flat front that propagates with constant speed. In this case it is possible to find an analytical solution of the nonlinear system. We call it zeroth-order solution and denote the functions with a superscript: $\left(T^{(0)}, \psi^{(0)}, H^{(0)}\right)$. For simplicity, we switch to a reference frame that moves with speed $C_0$. In the new frame the flat front is given by $H^{(0)} = 0$, so Eq. 2.15a becomes

$$\frac{\partial T}{\partial t} = \nabla^2 T + Q\delta(x) + C_0 \frac{\partial T}{\partial x}. \tag{2.17}$$

Changing reference frames introduces the last term in Eq. 2.17; the advection term $\mathbf{v} \cdot \boldsymbol{\nabla} T$ does not appear in it because we assumed that there is no fluid flow. The steady-state solution for the simplified heat equation is given by

$$T^{(0)} = \begin{cases} Q/C_0, & \text{for } x < 0, \\ (Q/C_0)e^{-C_0 x}, & \text{for } x \geq 0. \end{cases} \tag{2.18}$$

The Poisson equation for $\psi^{(0)}$ turns into a Laplace equation: $T^{(0)}$ and $H^{(0)}$ have no $y$-dependence, so both terms in the right-hand side of Eq. 2.15b vanish. Since the stream function is subjected to null boundary conditions, its zeroth-order solution takes the form $\psi^{(0)} = 0$, which is consistent with the assumption of no fluid flow ($\mathbf{v}^{(0)} = 0$).

In the next section, after developing the bases of linear stability analysis, we will perturb the base state and determine the conditions for the perturbations to grow or decay in time.

## 2.3 Linear Stability Analysis

Let us consider the simplest nontrivial dynamical system, in which the time evolution of a single variable is given by

$$\frac{\mathrm{d}u}{\mathrm{d}t} = f(u); \tag{2.19}$$

in general $f$ is a nonlinear function of $u$. We assume that this system has a stationary state $u^{(0)}$, for which both sides of the previous equation equal $0$. To probe the stability of this solution, we add a small perturbation $u^{(1)}$ to it. We introduce the perturbed solution in Eq. 2.19, and obtain

$$\frac{\mathrm{d}u^{(0)}}{\mathrm{d}t} + \frac{\mathrm{d}u^{(1)}}{\mathrm{d}t} = \frac{\mathrm{d}u^{(1)}}{\mathrm{d}t} = f\left(u^{(0)} + u^{(1)}\right). \tag{2.20}$$

Since $u^{(1)}$ is assumed to be small, we can Taylor-expand the last term in Eq. 2.20 to obtain

$$\frac{\mathrm{d}u^{(1)}}{\mathrm{d}t} = f\left(u^{(0)}\right) + u^{(1)} f'\left(u^{(0)}\right) + \ldots = u^{(1)} f'\left(u^{(0)}\right) + \ldots, \tag{2.21}$$

where $f'$ denotes the derivative of $f$ with respect to $u$ (evaluated at the stationary state) and the ellipses denote higher-order terms in $u^{(1)}$. If $f'\left(u^{(0)}\right) \neq 0$, these terms can be neglected [25]. After defining $\lambda \equiv f'\left(u^{(0)}\right)$, Eq. 2.21 becomes

$$\frac{\mathrm{d}u^{(1)}}{\mathrm{d}t} = \lambda u^{(1)}. \tag{2.22}$$

If $\lambda$ were positive, the solution would be a growing exponential, meaning that the system stops being in the steady state. If $\lambda$ were negative, the system would converge asymptotically to the steady state by virtue of the decaying exponential.

The previous procedure can be extended to higher-dimensional systems of $n$ unknowns $\mathbf{u}^T = (u_1, ..., u_n)$, which are functions of time and evolve according to

$$\frac{\mathrm{d}\mathbf{u}}{\mathrm{d}t} = \mathbf{F}\left(\mathbf{u}\right). \tag{2.23}$$

$\mathbf{F}$ is then linearized about a perturbed stationary state $\mathbf{u}^{(0)} + \mathbf{u}^{(1)}$ to obtain differential equations for the perturbations:

$$\frac{\mathrm{d}\mathbf{u}^{(1)}}{\mathrm{d}t} = \tilde{F} \cdot \mathbf{u}^{(1)}, \tag{2.24}$$

where the matrix $\tilde{F}$ stands for the linearization of $\mathbf{F}$. The solution of Eq. 2.24 can in principle be written as a linear combination of the eigenvectors of $\tilde{F}$, with the coefficients involving exponentials of the corresponding eigenvalues. This procedure can in turn be extended to unknowns that depend on more than one variable — see, for instance, [26].

We begin our linear stability analysis substituting the perturbed base state into our nonlinear system:

$$\begin{cases} \dfrac{\partial T^{(1)}}{\partial t} + \mathbf{v}^{(1)} \cdot \boldsymbol{\nabla}\left(T^{(0)} + T^{(1)}\right) = \nabla^2\left(T^{(0)} + T^{(1)}\right) \\ \qquad\qquad + Q\delta(x - H^{(1)}) + C_0\dfrac{\mathrm{d}T^{(0)}}{\mathrm{d}x} + C_0\dfrac{\partial T^{(1)}}{\partial x}, & \text{(2.25a)} \\ \qquad \nabla^2\psi^{(1)} = \mathrm{Ra_T}\dfrac{\partial T^{(1)}}{\partial y} + \mathrm{Ra_C}\dfrac{\partial H^{(1)}}{\partial y}\delta(x - H^{(1)}), & \text{(2.25b)} \\ \qquad \dfrac{\partial H^{(1)}}{\partial t} = \dfrac{1}{2}\left(\dfrac{\partial H^{(1)}}{\partial y}\right)^2 + \dfrac{1}{\mathscr{L}}\dfrac{\partial^2 H^{(1)}}{\partial y^2} + {v_x}^{(1)} - {v_y}^{(1)}\dfrac{\partial H^{(1)}}{\partial y}. & \text{(2.25c)} \end{cases}$$

Since $T^{(0)}$ satisfies

$$\nabla^2 T^{(0)} + C_0\frac{\mathrm{d}T^{(0)}}{\mathrm{d}x} + Q\delta(x) = 0, \tag{2.26}$$

we can plug this equality in Eq. 2.25a, cancel the first two terms (of Eq. 2.26), and rearrange to obtain

$$\frac{\partial T^{(1)}}{\partial t} + \mathbf{v}^{(1)} \cdot \boldsymbol{\nabla}\left(T^{(0)} + T^{(1)}\right) = \nabla^2 T^{(1)} - Q\delta(x) + Q\delta(x - H^{(1)}) + C_0\frac{\partial T^{(1)}}{\partial x}. \tag{2.27}$$

We would like to keep one delta-function term in order to have a heat source in our linear stability analysis. To this end, let us first recall that a function's derivative can be written as

$$\frac{\mathrm{d}f}{\mathrm{d}x} = \lim_{h\to 0} \frac{f(x) - f(x-h)}{h}. \tag{2.28}$$

The derivative of a delta function can be defined rigorously using distribution theory [27]. $H^{(1)}$ is a very small perturbation and, as we shall see, can decay to $0$ only in the limit $t \to \infty$. We therefore approximate all $\delta(x - H^{(1)})$ by $\delta'(x)$, the derivative of $\delta(x)$ with respect to $x$:

$$\delta(x - H^{(1)}) \approx \delta(x) - H^{(1)}\delta'(x). \tag{2.29}$$

After neglecting the terms nonlinear in $T^{(1)}$, $\psi^{(1)}$, or $H^{(1)}$ and simplifying we obtain the linearized system

$$\begin{cases} \dfrac{\partial T^{(1)}}{\partial t} + \mathbf{v}^{(1)} \cdot \boldsymbol{\nabla} T^{(0)} = \nabla^2 T^{(1)} - Q H^{(1)} \delta'(x) + C_0 \dfrac{\partial T^{(1)}}{\partial x}, & \text{(2.30a)} \\ \nabla^2 \psi^{(1)} = \mathrm{Ra_T} \dfrac{\partial T^{(1)}}{\partial y} + \mathrm{Ra_C} \dfrac{\partial H^{(1)}}{\partial y} \delta(x), & \text{(2.30b)} \\ \dfrac{\partial H^{(1)}}{\partial t} = \dfrac{1}{\mathscr{L}} \dfrac{\partial^2 H^{(1)}}{\partial y^2} + {v_x}^{(1)}. & \text{(2.30c)} \end{cases}$$

We will now perturb the base state solution of the previous section expressing the perturbations with Fourier series. Let us recall that $\partial H/\partial y$, $\partial T/\partial y$, and $\psi$ equal $0$ at the tube's walls. This allows us to use sine or cosine functions accordingly to match the boundary conditions:

$$\begin{cases} T^{(1)} = \displaystyle\sum_q T_q(x,t)\cos(qy), & \text{(2.31a)} \\ \psi^{(1)} = \displaystyle\sum_q \psi_q(x,t)\sin(qy), & \text{(2.31b)} \\ H^{(1)} = \displaystyle\sum_q H_q(t)\cos(qy). & \text{(2.31c)} \end{cases}$$

Finally, after substituting single modes in Eqs. 2.30, dropping the subscripts, and simplifying, we obtain a linear system:

$$\begin{cases} \dfrac{\partial T}{\partial t} = \dfrac{\partial^2 T}{\partial x^2} - q^2 T - q\psi \dfrac{\mathrm{d}T^{(0)}}{\mathrm{d}x} - QH\delta'(x) + C_0 \dfrac{\partial T}{\partial x}, & \text{(2.32a)} \\ \dfrac{\partial^2 \psi}{\partial x^2} = q^2\psi - q\left[\mathrm{Ra_T} T + \mathrm{Ra_C} H \delta(x)\right], & \text{(2.32b)} \\ \dfrac{\mathrm{d}H}{\mathrm{d}t} = \dfrac{-q^2}{\mathscr{L}} H + q\psi|_{x=0}. & \text{(2.32c)} \end{cases}$$

The solutions to the linearized system can be found by looking for functions of the form $T = T(x)e^{\sigma t}$, $\psi = \psi(x)e^{\sigma t}$, $H = \tilde{H}e^{\sigma t}$. For each value of the wavenumber $q$ we obtain an eigenvalue system for the growth rate $\sigma$. Therefore, perturbations will decay to zero if all the growth rates have negative real parts — i.e., the system will be stable

when subjected to those perturbations. In contrast, if at least one growth rate has a positive real part, the perturbations will grow exponentially and destabilize the base state $\left(T^{(0)}, \psi^{(0)}, H^{(0)}\right)$. This would result in different types of non-flat convective fronts. Instead of solving the eigenvalue equation we start with a small perturbation and let it evolve using Eqs. 2.32. After sufficient time has ellapsed, the term with the dominating eigenvalue — be it positive or negative — takes over $T^{(1)}, \psi^{(1)}$, and $H^{(1)}$. We can then fit these functions as exponentials and calculate said eigenvalue, as we will explain in the next section.

# 3. Numerical methods

The nonlinear and linear systems — Eqs. 2.15 and 2.32, respectively — were solved numerically using finite-differences schemes. We discretized our computational domain using a two-dimensional grid $(x_i, y_j)$ of mesh length $\Delta x$ and width $\Delta y$; our unknown functions evolved in discrete time steps $t_n = n\Delta t$. This way, we expressed the discrete temperature as $T^n_{i,j} \equiv T(x_i, y_j, t_n)$ and wrote the other functions in a similar manner. All derivatives were discretized via finite-differences approximations to second order in position, for example

$$\frac{\partial^2 T}{\partial x^2} \to \frac{T^n_{i+1,j} - 2T^n_{i,j} + T^n_{i-1,j}}{\Delta x^2}, \tag{3.1}$$

and first order in time,

$$\frac{\partial T}{\partial t} \to \frac{T^{n+1}_{i,j} - T^n_{i,j}}{\Delta t}. \tag{3.2}$$

The corresponding uncertainties were $\mathcal{O}(\Delta x^2)$, $\mathcal{O}(\Delta y^2)$, and $\mathcal{O}(\Delta t)$ [28].

Since real computational domains cannot have infinite extension, we restricted ours to the set of points $\{(x, y) : [-Lx, Lx] \times [0, Ly]\}$, where $Lx$ and $Ly$ are the tube's half-length and width, respectively. The grid representing this domain consisted of $2\,nx \times ny$ points; $nx$ and $ny$ were varied in order to keep the dimensions of the mesh rectangles constant at $\Delta x = Lx/nx = 6.25 \times 10^{-2}$ and $\Delta y = Ly/ny = 4.54 \times 10^{-2}$. Numerical stability constrained the uncertainties to satisfy the inequality

$$\Delta t \left( \frac{1}{\Delta x^2} + \frac{1}{\Delta y^2} \right) \leq \frac{1}{2}, \tag{3.3}$$

in order for the numerical scheme of the diffusion equation to work — see Ref. [29]. With this restriction and the previous values of $\Delta x$ and $\Delta y$ in mind, we set $\Delta t = 5 \times 10^{-4}$.

For the nonlinear calculations we Euler-integrated forward in time Eqs. 2.15a and 2.15c — computing $T^{n+1}_{i,j}$ and $H^{n+1}_j$ in each time step — until a steady state was reached. In some cases the solutions converged, whereas in others they presented small oscillations ranging from $\mathcal{O}(10^{-5})$ to $\mathcal{O}(10^{-9})$. Since these fluctuations were much smaller than the uncertainties, e.g. $\Delta x^2 = 3.91 \times 10^{-3}$, we neglected them. The subroutine GENBUN from the FISHPAK package [30] solved directly the discretized version of the Laplace equation for $\psi$, Eq. 2.15b. To verify the consistency of our

solutions we computed and compared both sides of Eqs. 2.15 at arbitrary times using the previously obtained solutions.

In order to write an algorithm for any equation, we must specify a finite computational domain beforehand. As time passes, the singularity of the delta function in Eq. 2.15a shifts further away along the $x$-axis — we would need to declare an enormous domain. This would slow down the computations. We avoided this problem switching to a system that moves with a given speed $u(t)$, such that in the new frame $H$ is always centered at $x = 0$. In practice the front's shape and speed will vary until the system reaches a steady state. For our calculations we set $u(t)$ equal to the speed of the average front position.

To implement the delta function in two spatial dimensions we employed the Poisson kernel, which is given by

$$\delta\left(x - H\right) = \lim_{\epsilon \to 0} \frac{1}{\pi} \frac{\epsilon}{\left(x - H\right)^2 + \epsilon^2}. \tag{3.4}$$

This representation assigns a number to each point in the grid. The assigned values drop drastically as we move away from $x = H$ because points outside the front release no heat. In order to use Eq. 3.4, we had to tune $\epsilon$ via trial and error. Since this parameter represents the length scale in which the discrete delta function decays away from $H$, we used $\Delta x$ and $\Delta y$ as references to find the correct tuning value and found that $\epsilon = 6.25 \times 10^{-2}$ gave the best fit to the base state.

For the linear stability analysis, we solved the discretized versions of Eqs. 2.30a and 2.30c via Euler-integration. The linearized Poisson equation for the stream function, Eq. 2.30b, called for a different approach: a relaxation scheme [31] calculated $\psi^{(1)}$ at every time step. To implement $\delta'(x)$ we used the rectangular function suggested in Ref. [32].

When solving the linear system, we could not always expect everything to converge: if the real part of the growth rate were positive, the perturbations would grow indefinitely. Instead, we ran the programs until the largest eigenvalue dominated completely the growth or decay. Once it did, the perturbations would have a time dependence of $e^{\sigma t}$. Then we would be able to fit the solutions as exponential functions. To do this we took three values of $T$ at different times, and computed the growth rate that the perturbation would have if these points described an exponential function. This quantity eventually converged, indicating that the perturbation was dominated by the largest eigenvalue.

To model the iodate-arsenous acid reaction, we set the diffusivities $D_T = 1.45 \times 10^{-3}\mathrm{cm}^2/\mathrm{s}$ and $D_C = 2 \times 10^{-5}\mathrm{cm}^2/\mathrm{s}$, using the same parameters as Edwards *et al.* [21]. As a consequence, the Lewis number took the value $\mathscr{L} = 72.5$.

Both systems were solved using codes written in FORTRAN 90. After compiling the codes, we submitted the resulting programs to the computational unit of the university's Physics Department. The execution times of the nonlinear calculations ranged from half an hour to almost two days, depending on the tube's dimensions. On the other hand, the programs that solved the linear system were each completed in less than twenty minutes.

# 4. Results and discussion

## 4.1 Flat-Front Stability Analysis

We carried out a linear stability analysis to probe the importance of thermal gradients. To do this, we fixed $\mathrm{Ra_C} = 0.0$ and varied $\mathrm{Ra_T}$ over a positive range of values. As we previously discussed, perturbations to the front grow or decay exponentially as $e^{\sigma t}$ — where $\sigma$ corresponds to the the growth rate with the largest real part — after sufficient time has ellapsed. Our results are summarized in Fig. 4.1. To understand this figure, we must first note that

- if $\mathrm{Re}[\sigma(q)] > 0$, the perturbations grow and destabilize the flat front — the quadratic term in the front equation (Eq. 2.15c) halts this growth, resulting in the steady states presented in the following section;
- but if $\mathrm{Re}[\sigma(q)] < 0$, the perturbations wane in time, which means that the flat front remains stable.

We see then that, as thermal density gradients — represented by larger $\mathrm{Ra_T}$ — increase, the flat front becomes unstable to perturbations of larger wavenumbers $q$. Tubes of width $Ly < \pi/q$ filter out perturbations of wavelength larger than $Ly$, i.e., of wavenumber smaller than $q$. Therefore, only large wavenumbers are allowed in sufficiently narrow tubes, which according to Fig. 4.1 results in growth rates with negative real part — flat fronts will be stable in narrow tubes. As thermal gradients strengthen, the tubes allowing stable flat fronts will need to be more narrow because the range of unstable perturbations increases.

Given positive composition Rayleigh numbers — which indicate inherently unstable configurations because the fluid on top is denser than the one below — we expect non-flat fronts to develop. The dispersion curves A and B in Fig. 4.2a — corresponding to $\mathrm{Ra_C} = 0.3$, $\mathrm{Ra_T} = 2.0$ and $\mathrm{Ra_C} = 0.1$, $\mathrm{Ra_T} = 0.75$, respectively — show that curved fronts appear at values of $Ly = \pi/q < 1$. In general, the wavenumber of a perturbation determines the stability of a front. Nevertheless, we also found that if the thermal gradient is reversed, the system can be stable: for sufficiently negative $\mathrm{Ra_T}$, the real part of the growth rate can be negative for all $q$. We observe this behavior in curves

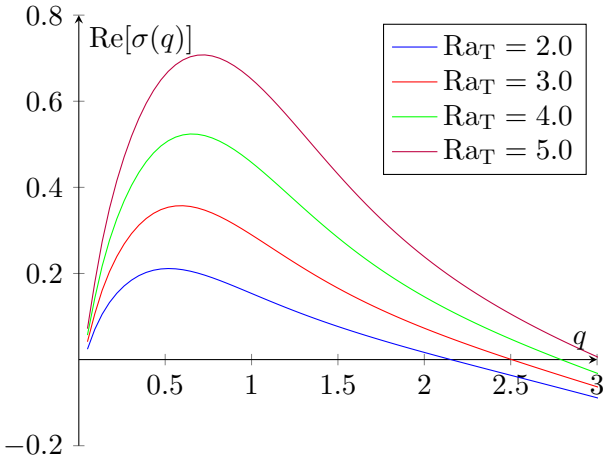


Figure 4.1: The perturbations' growth rates as functions of the wavenumber, for different values of $\mathrm{Ra_T}$ and $\mathrm{Ra_C} = 0.0$. In tubes of width greater than or equal to a critical value — corresponding to the wavenumber at which $\mathrm{Re}[\sigma(q)]$ changes sign — the perturbations grow and destabilize the flat front.

C ($\mathrm{Ra_C} = 0.0$, $\mathrm{Ra_T} = -0.5$) and D ($\mathrm{Ra_C} = 0.1$, $\mathrm{Ra_T} = -2.0$). In curve E ($\mathrm{Ra_C} = 0.4$, $\mathrm{Ra_T} = -1.5$) the compositional gradient has overpowered its thermal counterpart, thus disrupting the previously mentioned stability.

We obtain unconditionally stable configurations when both $\mathrm{Ra_T}$ and $\mathrm{Ra_C}$ are negative, as shown in curves F ($\mathrm{Ra_C} = -0.05$, $\mathrm{Ra_T} = -0.25$) and G ($\mathrm{Ra_C} = -0.1$, $\mathrm{Ra_T} = -1.5$) of Fig. 4.2b. Edwards *et al.* [21] argued that sufficiently strong thermal gradients could ignite convection in configurations where the lighter fluid is on top of the heavier one, i.e., in systems with $\mathrm{Ra_C} < 0$. Curves H ($\mathrm{Ra_C} = -0.2$, $\mathrm{Ra_T} = 2.5$) and I ($\mathrm{Ra_C} = -0.1$, $\mathrm{Ra_T} = 0.75$) confirm this conjecture: the growth rates are positive in a range of wavenumbers and negative outside of it, recovering the behavior observed in Fig. 4.1.

Finally, we summarize this section's results using the parameter space spanned by the Rayleigh numbers, as D'Hernoncourt *et al.* did in Refs. [33] and [34]. We define the Rayleigh plane as the set of points with coordinates $(\mathrm{Ra_C}, \mathrm{Ra_T})$. Figure 4.3 shows this plane in the domain we covered in our linear stability analysis. The instability region contains the unstable configurations of the system and is colored red; points in the stability region, colored blue, represent systems where flat fronts are stable. The first quadrant corresponds to entirely unstable configurations. In the third quadrant, both Rayleigh numbers are negative and the fronts are always stable. Configurations in the second and fourth quadrants of the plane will allow flat fronts depending on the values of the Rayleigh numbers.

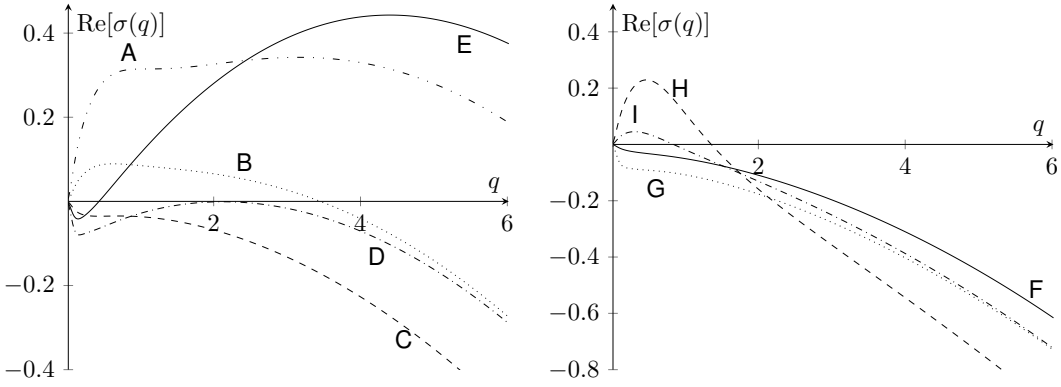


(a) Curve A corresponds to $\mathrm{Ra_C} = 0.3$ and $\mathrm{Ra_T} = 2.0$; curve B to $\mathrm{Ra_C} = 0.1$ and $\mathrm{Ra_T} = 0.75$; curve C to $\mathrm{Ra_C} = 0.0$ and $\mathrm{Ra_T} = -0.5$; curve D to $\mathrm{Ra_C} = 0.1$ and $\mathrm{Ra_T} = -2.0$; and curve E to $\mathrm{Ra_C} = 0.4$ and $\mathrm{Ra_T} = -1.5$.

(b) Curve F corresponds to $\mathrm{Ra_C} = -0.05$ and $\mathrm{Ra_T} = -0.25$; curve G to $\mathrm{Ra_C} = -0.1$ and $\mathrm{Ra_T} = -1.5$; curve H to $\mathrm{Ra_C} = -0.2$ and $\mathrm{Ra_T} = 2.5$; and curve I to $\mathrm{Ra_C} = -0.1$ and $\mathrm{Ra_T} = 0.75$.

Figure 4.2: Dispersion relations for different combinations of $\mathrm{Ra_T}$ and $\mathrm{Ra_C}$.

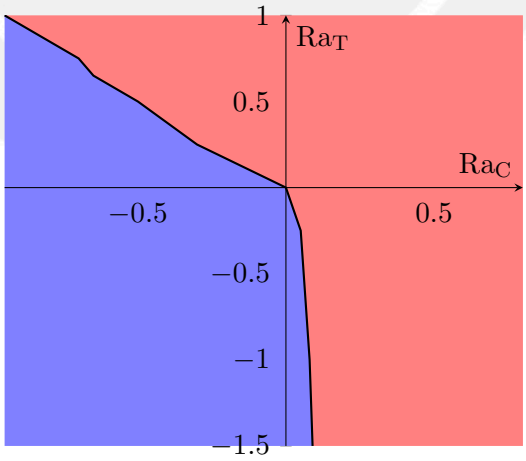


Figure 4.3: The red region in the Rayleigh plane corresponds to situations in which the perturbation wavenumber determines whether the flat front is stable or unstable; configurations in the blue region are unconditionally stable.

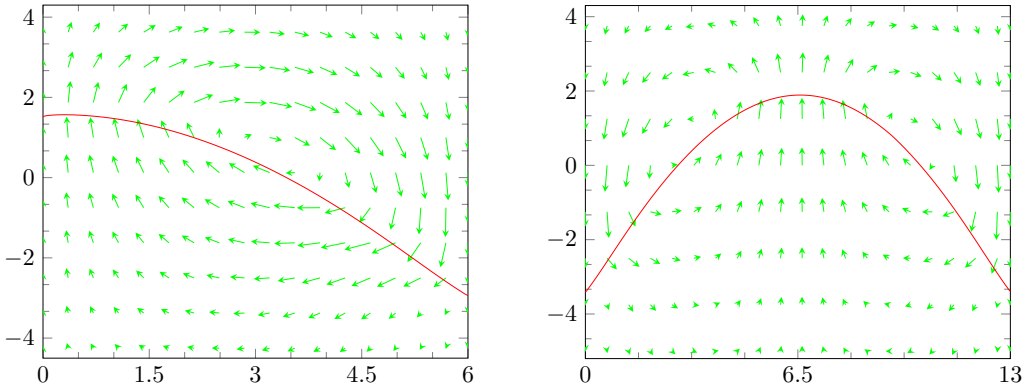


(a) Fluid velocity field and $H$, $Ly = 6.0$

(b) Fluid velocity field and $H$, $Ly = 13.0$

Figure 4.4: The steady-state non-axisymmetric and axisymmetric fronts for $Ly = 6.0$ and $Ly = 13.0$, respectively, in their velocity fields. The abscissas and ordinates correspond to the horizontal and vertical directions, respectively.

## 4.2 Nonlinear System

We explored the front's behavior at the onset of convection by solving the full set of nonlinear equations, Eqs. 2.15. The effects of thermal gradients on front propagation interested us; therefore, we studied our nonlinear system without considering compositional effects. Since we aimed to study reaction fronts not far from the onset of convection, the fluid velocity and the spatial derivatives of the front height function were taken to be small. The product of these two quantities would be smaller than both, so we neglected the last term in Eq. 2.15c. The nonlinear simulations were carried out using $\mathrm{Ra_C} = 0.0, \mathrm{Ra_T} = 3.0$, and $Q = 1$ and yielded three types of fronts:

- a flat front in tubes of width $Ly < 1.26$,
- a non-axisymmetric front when $1.26 \leq Ly < 12.8$, and
- an axisymmetric front for $Ly \geq 12.8$.

We stress that the tube width at which the front transitions from flat to non-axisymmetric coincides with the results of the linear stability analysis (see Fig. 4.1).

As Figs. 4.4a and 4.4b show, in the non-axisymmetric case the fluids rise on one side of the tube and fall on the other, whereas in the axisymmetric case they rise at the center and fall on the sides. Previous theoretical works — which accounted only for compositional density gradients and excluded thermal effects — showed that flat fronts become non-axisymmetric at the onset of convection [35] and that these fronts shift to the axisymmetric mode in presence of stronger convective effects [36]. These predictions, which did not account for finite thermal diffusivities, agree with the experimental findings of Masere *et al.* [16]. The non-axisymmetric fronts we obtained

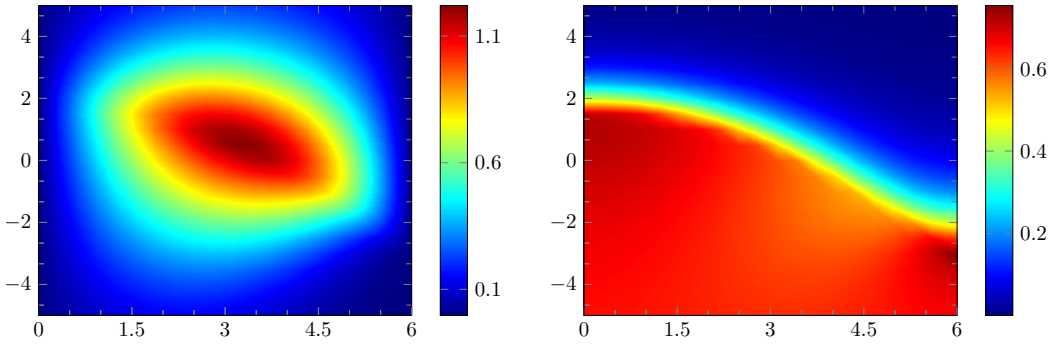


(a) Steady state $\psi$, $Ly = 6.0$ (b) Steady state $T$, $Ly = 6.0$

Figure 4.5: Color maps of the steady-state stream function and temperature for $Ly = 6.0$. The abscissas and ordinates correspond to the horizontal and vertical directions, respectively.

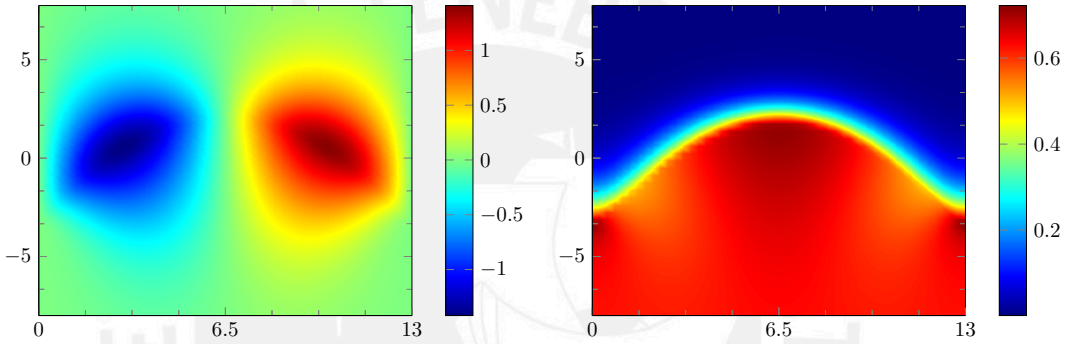


(a) Steady state $\psi$, $Ly = 13.0$ (b) Steady state $T$, $Ly = 13.0$

Figure 4.6: Color maps of the steady-state stream function and temperature for $Ly = 13.0$. The abscissas and ordinates correspond to the horizontal and vertical directions, respectively.

have no local extrema — their only extrema occur at the boundaries, as in Fig. 4.4a — whereas their counterparts in the previous reference do have a local maximum near the center.

Figure 4.5 displays color maps of $T$ and $\psi$ in a tube of width $Ly = 6.0$, corresponding to non-axisymmetric convection. Accordingly, Fig. 4.6 shows the corresponding variables but for the axisymmetric case ($Ly = 13.0$). The qualitative features of all non-axisymmetric fronts resemble the results in Fig. 4.5; similarly, fronts in the axisymmetric regime resemble Fig. 4.6. The steady-state stream functions shown in Figs. 4.5a and 4.6a forecast, via Eq. 2.6, convection rolls in the velocity field; we therefore call them convection rolls too. In most cases corresponding to the non-axisymmetric mode we found $\psi$-surfaces with one roll, whereas two rolls were present in the axisymmetric mode. In both cases the temperature profiles show pronounced peaks near the fronts' extrema — heat concentrates in these zones, which are colored dark-red in Figs. 4.5b

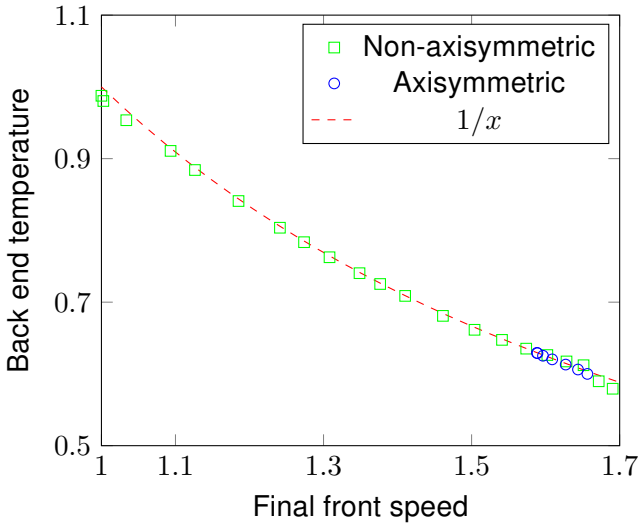


Figure 4.7: The back end temperature in the steady state is inversely proportional to the front speed. When the front becomes axisymmetric, the speeds drop and the back end temperatures rise, which results in a few points' overlapping. The speeds are measured in the laboratory frame.

and 4.6b.

The zeroth-order temperature, Eq. 2.18, predicts that, in absence of convection, the temperature below the front would be inversely proportional to the front speed. Since convection increases the front speed, it is interesting to observe how the temperature changes due to this increase in speed. We could still expect a $1/u$-dependence at the bottom of the tube because convective effects decay exponentially in the vertical direction — as seen, for example, in Ref. [21]. The results plotted in Fig. 4.7 confirm our forecast: the temperature at the back end of the tube, in the axisymmetric and non-axisymmetric branches, is inversely proportional to the speed enhanced by convection.

To get a quantitative idea of how much the front deviates from flatness, we computed the variance of the discrete front using the formula

$$\mathrm{Var}(t_n) = \frac{\sum_j \left(H_j^n - \bar{H}^n\right)^2}{ny}, \tag{4.1}$$

where, at time $t_n$, $\bar{H}^n$ is the average position of $H$, $H_j^n = H(y_j, t_n)$ the discrete front, and $ny$ the number of points. We computed the right-hand side of Eq. 2.15c to calculate the front speed; all points had the same speed in the steady state. By virtue of the curvature term in the eikonal relation, the upper parts of the fronts in Figs. 4.4a and 4.4b should move with speed less than $C_0$. The fluid velocity, however, tends to raise these parts and eventually overcomes the curvature term. Our results show that, as the fronts become more curved, they move faster: Figures 4.8a and 4.8b show that the

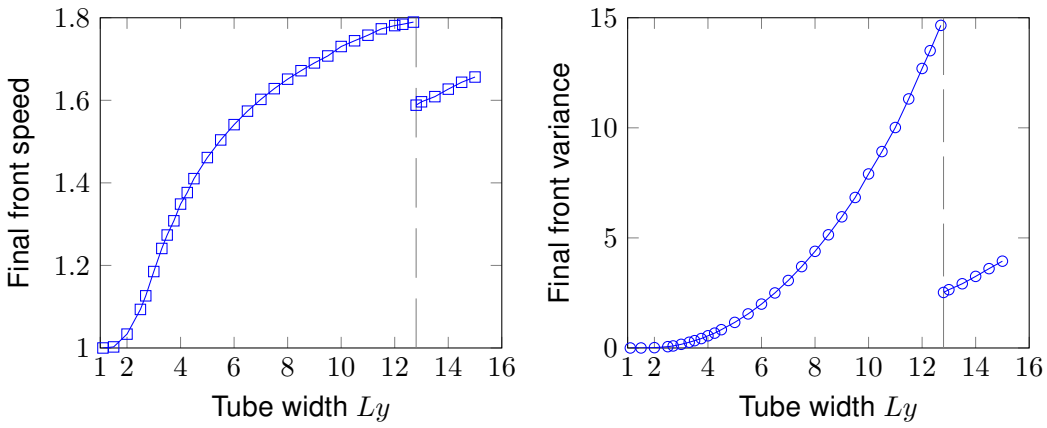


(a) Steady-state speed vs. tube width

(b) Steady-state variance vs. tube width

Figure 4.8: The steady-state front speed and variance in are larger in wider tubes. The curves break at $Ly = 12.8$, when the front transits from non-axisymmetric to axisymmetric.

front speed and variance increased with the tube width. At $Ly = 12.8$ both parameters drop, signaling the change to the axisymmetric mode. Increasing the tube width further, we observe a corresponding increase in front speed and variance.

# 5. Conclusions

We have presented a nonlinear system of equations that describe how the temperature, velocity field, and front height in a chemical reaction evolve in time. This model accounts for both thermal and chemical composition gradients. Perturbing the system's flat front solution and carrying out a linear stability analysis on it gave us a linearized system for the time evolution of the perturbations. The computational algorithms we devised solved both systems employing various well-known numerical schemes.

Our nonlinear model yielded three types of front — flat, non-axisymmetric, and axisymmetric — which resemble previous results obtained in models that neglected thermal effects. The temperature at the back-end of the tube behaved as predicted by the flat-front solution of the heat equation in spite of convective effects. The plots of steady-state speed and variance as functions of the tube width indicate that the eikonal relation has coupled correctly in our model. The results of the stability analysis divided the Rayleigh plane — the parameter space of the Rayleigh numbers — in two regions: the stability region, in which flat fronts remain undisturbed, and the instability region, where non-axisymmetric and axisymmetric fronts develop. Depending on the sign of $\mathrm{Ra_T}$, sufficiently strong thermal gradients can either disrupt otherwise stable configurations or stabilize inherently unstable configurations.

Our nonlinear results resemble those presented in Ref. [16]. Only the non-axisymmetric fronts are distinctly different from the ones in said reference — this is to be expected because those results were obtained in a cylindrical geometry. Solving the system at larger tube widths could reveal new convective front modes. Given the available computational resources, however, it would take days to solve Eqs. 2.15 for higher values of $nx$ and $ny$.

Solving for $H$ caused some computational difficulties: the discretized version of Eq. 2.15c required that we used a small $\Delta t$ — unlike reaction-diffusion systems, which can be modelled using time steps of $\Delta t \sim 1$. We suggest solving the heat and front equations employing a Runge-Kutta scheme. This way, a time step as small as ours would not be needed, which would reduce significantly the computation time (at the cost of having to implement a more complex algorithm).

Working with the parameters corresponding to the iodate-arsenous acid reaction, we have shown the applicability of our model for autocatalytic reaction fronts. If we were to choose different thermal and molecular diffusivities (characteristic of other reactions), we would obtain different Lewis numbers — for example, the chlorite-tetrathionate reaction is characterized by a Lewis number $\mathscr{L} \sim 10$. Exploring further regions of the Rayleigh plane for the iodate-arsenous acid reaction or any other autocatalytic reaction could yield instability regions that, counterintuitively, do not occupy the full extent of the third quadrant. This would indicate the presence of more complex phenomena such as double-diffusive processes [37].

# Bibliography

[1]M. B. Short, P. J. Brantingham, A. L. Bertozzi, and G. E. Tita, "Dissipation and displacement of hotspots in reaction-diffusion models of crime", *P. Natl. Acad. Sci. USA* **107**, 3961–3965 (2010).

[2]E. N. Lorenz, "Deterministic nonperiodic flow", *J. Atmos. Sci.* **20**, 130–141 (1963).

[3]R. Lefever, N. Barbier, P. Couteron, and O. Lejeune, "Deeply gapped vegetation patterns: On crown/root allometry, criticality and desertification", *J. Theor. Biol.* **261**, 194–209 (2009).

[4]D. Cumin and C. Unsworth, "Generalising the Kuramoto model for the study of neuronal synchronisation in the brain", *Physica D* **226**, 181–196 (2007).

[5]J. A. Pojman and I. R. Epstein, "Convective effects on chemical waves. 1. Mechanisms and stability criteria", *J. Phys. Chem.* **94**, 4966–4972 (1990).

[6]J. D'Hernoncourt and A. D. Wit, "Influence of heat losses on nonlinear fingering dynamics of exothermic autocatalytic fronts", *Physica D* **239**, 819–830 (2010).

[7]K. Showalter, "Quadratic and cubic reaction-diffusion fronts", *Nonlinear Sci. Today* **4**, 1–2 (1994).

[8]P. Kolodner, "Drifting pulses of traveling-wave convection", *Phys. Rev. Lett.* **66**, 1165–1168 (1991).

[9]O. Singh, D. Ranjan, J. Srinivasan, and K. Sreenivas, "A study of basalt fingers using experiments and numerical simulations in double-diffusive systems", *J. Geogr. Geol.* **3**, 42–50 (2011).

[10]D. R. Stegman, A. M. Jellinek, S. A. Zatman, J. R. Baumgardner, and M. A. Richards, "An early lunar core dynamo driven by thermochemical mantle convection", *Nature* **421**, 143–146 (2003).

[11]J. T. H. Andres and S. S. S. Cardoso, "Onset of convection in a porous medium in the presence of chemical reaction", *Phys. Rev. E* **83**, 046312 (2011).

[12]A. Hanna, A. Saul, and K. Showalter, "Detailed studies of propagating fronts in the iodate oxidation of arsenous acid", *J. Am. Chem. Soc.* **104**, 3838–3844 (1982).

[13]A. Saul and K. Showalter, in *Oscillations and Traveling Waves in Chemical Systems* (Wiley-Interscience, 1985) Chap. Propagating reaction-diffusion fronts, pp. 419–439.

[14]Y. M. Sternberg and V. H. Scott, "The Hele-Shaw Model: A Research Device in Ground-Water Studies", *Ground Water* **2**, 33–37 (1964).

[15]J. W. Wilder, B. F. Edwards, and D. A. Vasquez, “Finite thermal diffusivity at onset of convection in autocatalytic systems: continuous fluid density”, *Phys. Rev. A* **45**, 2320–2327 (1992).

[16]J. Masere, D. A. Vasquez, B. F. Edwards, J. W. Wilder, and K. Showalter, “Nonaxisymmetric and axisymmetric convection in propagating reaction-diffusion fronts”, *J. Phys. Chem.* **98**, 6505–6508 (1994).

[17]D. A. Vasquez, B. F. Edwards, and J. W. Wilder, “Finite thermal diffusivity at onset of convection in autocatalytic systems: Discontinuous fluid density”, *Phys. Fluids* **7**, 2513–2515 (1995).

[18]S. Kalliadasis, J. Yang, and A. De Wit, “Fingering instabilities of exothermic reaction-diffusion fronts in porous media”, *Phys. Fluids* **16**, 1395–1409 (2004).

[19]J. D’Hernoncourt, S. Kalliadasis, and A. De Wit, “Fingering of exothermic reaction-diffusion fronts in Hele-Shaw cells with conducting walls”, *J. Chem. Phys.* **123** (2005).

[20]T. Gérard, T. Tóth, P. Grosfils, D. Horváth, A. De Wit, and A. Tóth, “Hot spots in density fingering of exothermic autocatalytic chemical fronts”, *Phys. Rev. E* **86**, 016322 (2012).

[21]B. F. Edwards, J. W. Wilder, and K. Showalter, “Onset of convection for autocatalytic reaction fronts: Laterally unbounded system”, *Phys. Rev. A* **43**, 749–760 (1991).

[22]E. A. Spiegel and G. Veronis, “On the Boussinesq approximation for a compressible fluid”, *Astrophys. J.* **131**, 442–447 (1960).

[23]D. J. Griffiths, *Introduction to Electrodynamics* (Prentice-Hall, 1999).

[24]J. W. Wilder, B. F. Edwards, D. A. Vasquez, and G. I. Sivashinsky, “Derivation of a nonlinear front evolution equation for chemical waves involving convection”, *Physica D* **73**, 217–226 (1994).

[25]S. H. Strogatz, *Nonlinear Dynamics and Chaos: With Applications to Physics, Biology, Chemistry, and Engineering*, Studies in Nonlinearity (Perseus Books, 1994).

[26]M. C. Cross and P. C. Hohenberg, “Pattern formation outside of equilibrium”, *Rev. Mod. Phys.* **65**, 851–1112 (1993).

[27]A. Zolotaryuk, “Boundary conditions for the states with resonant tunnelling across the $\delta'$-potential”, *Phys. Lett. A* **374**, 1636–1641 (2010).

[28]S. E. Koonin and D. C. Meredith, *Computational Physics: Fortran Version*, The Advanced Book Program (Addison-Wesley, 1994).

[29]C. A. J. Fletcher, *Computational Techniques for Fluid Dynamics. Volume 1. Fundamental and General Techniques*, Springer Series in Computational Physics (Springer-Verlag, Berlin, 1991).

[30]P. N. Swarztrauber and R. A. Sweet, “Algorithm 541: Efficient Fortran subprograms for the solution of separable elliptic partial differential equations [D3]”, *ACM Trans. Math. Softw.* **5**, 352–364 (1979).

[31]W. H. Press, S. A. Teukolsky, W. T. Vetterling, and B. P. Flannery, *Numerical Recipes in Fortran 77: The art of scientific computing. Volume 1 of Fortran Numerical Recipes* (Cambridge University Press, 1997).

[32]D. J. Griffiths, “Boundary conditions at the derivative of a delta function”, *J. Phys. A: Math. Gen.* **26**, 2265 (1993).

[33]J. D’Hernoncourt, A. Zebib, and A. De Wit, “Reaction driven convection around a stably stratified chemical front”, *Phys. Rev. Lett.* **96**, 154501 (2006).

[34]J. D’Hernoncourt, A. De Wit, and A. Zebib, “Double-diffusive instabilities of autocatalytic chemical fronts”, *J. Fluid Mech.* **576**, 445–456 (2007).

[35]D. A. Vasquez, J. W. Wilder, and B. F. Edwards, “Convective instability of autocatalytic reaction fronts in vertical cylinders”, *Phys. Fluids A* **4**, 2410–2414 (1992).

[36]D. A. Vasquez, B. F. Edwards, and J. W. Wilder, “Onset of convection for autocatalytic reaction fronts: Laterally bounded systems”, *Phys. Rev. A* **43**, 6694–6699 (1991).

[37]T. Gérard and A. De Wit, “Stability of exothermic autocatalytic fronts with regard to buoyancy-driven instabilities in presence of heat losses”, *Wave Motion* **48**, 814–823 (2011).